Inelastic neutron scattering investigations of the quantum molecular dynamics of a H_{2} molecule entrapped inside a fullerene cage

A. J. Horsewill, K. S. Panesar, S. Rols, J. Ollivier, M. R. Johnson, M. Carravetta, S. Mamone, M. H. Levitt, Y. Murata, K. Komatsu, J. Y.-C. Chen, J. A. Johnson, X. Lei, and N. J. Turro

Inelastic neutron scattering investigations of the quantum molecular dynamics of a H₂ molecule entrapped inside a fullerene cage

A.J. Horsewill[*1], K.S. Panesar[1], S. Rols[2], J. Ollivier[2], M.R. Johnson[2], M. Carravetta[3], S. Mamone[3], M.H. Levitt[3], Y. Murata[4], K. Komatsu[4], J.Y.-C. Chen[5], J.A. Johnson[5], X. Lei[5], and N.J. Turro[5]

[1]School of Physics & Astronomy, University of Nottingham, Nottingham, NG7 2RD, UK

[2] Institut Laue-Langevin, BP 156, 38042 Grenoble, France

[3] School of Chemistry, University of Southampton, Southampton, SO17 1BJ, UK

[4] Institute for Chemical Research, Kyoto University, Kyoto 611-0011, Japan

[5] Department of Chemistry, Columbia University, New York, New York 10027, USA

[*]Corresponding author: email a.horsewill@nottingham.ac.uk

FAX +44 (0) 115 9515180

Abstract

The quantum dynamics of dihydrogen molecules entrapped inside fullerene cages has been investigated using inelastic neutron scattering (INS). For the endofullerene $H_2@C_{60}$ the low-lying energy levels of the manifold of coupled translational and rotational states have been accurately determined by studying INS spectra recorded in the temperature range $1.5 \leq T \leq 240 \text{ K}$. The majority of transitions observed in the INS spectra interconvert the nuclear spin isomers orthohydrogen and parahydrogen. The cage potential has icosahedral symmetry and splittings observed in the INS spectra reveal the coupling of translational and rotational angular momentum of the H_2 molecules. The effects of nuclear spin symmetry, isotope mass effects and cage anisotropy have been further investigated by studying $HD@C_{60}$ and H_2 inside an open cage endofullerene. The momentum transfer κ arising from the neutron scattering event has also been investigated. The κ-dependence spectra reflect the physical dimensions of the dihydrogen molecule and its confinement in its cage. We show how this may be used as a tool for assigning the INS transitions.

1. Introduction

At the heart of quantum mechanics is the concept of a particle trapped by a confining potential. Indeed the concept of wavelike orbitals relating to the motion of electrons in the electrostatic field of atoms and molecules is ubiquitous to the field of quantum chemistry. Less common is the entrapment of more massive particles such as atoms and molecules. Here the significantly larger mass means a much shorter de Broglie wavelength requiring proportionally smaller confinement regions to enable the quantization effects associated with centre of mass displacements to be measurable. In recent years some fascinating supramolecular complexes have been synthesized that provide a practical example of such an entrapped molecule. These are the hydrogen endofullerenes where a molecule of hydrogen is permanently encapsulated inside the cage formed by a fullerene molecule. [1,2,3] Of this family, the $H_2@C_{60}$ complex is the model system, displaying a highly symmetric cage potential.

The synthesis of these complexes is sophisticated, requiring a series of controlled reactions to open and stabilize an orifice in a fullerene molecule, whereupon a hydrogen molecule is inserted inside at high temperature and pressure. A further series of reactions reseals the orifice, lending the phrase 'molecular surgery' to the synthetic techniques [1,2]. A variety of small molecules have been encapsulated inside fullerenes, including the recent synthesis of $H_2O@C_{60}$ [4].

Komatsu and colleagues from Kyoto University [1,2] have pioneered and refined the synthesis making macroscopic samples available for investigation by a variety of experimental techniques. In addition to the increasing literature on the chemical principles [5,6,7,8,9,10,11,12], spectroscopic investigations using infra-red (IR) [3,13,14,15], inelastic neutron scattering (INS) [3,16,17] and nuclear magnetic resonance (NMR) [3,18,19] have probed the physical characteristics of these complexes. Also, heat capacity measurements have identified a small splitting of the rotational line associated with the symmetry of the crystal field, a first indication of inter-fullerene contributions to the effective cage potential [20]. IR and INS exhibit discrete line spectra that reveal the quantization of energy and angular momentum of the hydrogen molecule, assisting a deep understanding of the quantum dynamics of the entrapped molecule. NMR has facilitated the exploration of the particle dynamics at lower energies. Important quantum features also arise as a result of the Pauli exclusion principle (PEP) which leads directly to the identification of the nuclear spin-isomers para-hydrogen (p-H_2) and ortho-hydrogen (o-H_2). This entanglement of

3

space and spin variables has a dramatic influence on the quantum dynamics and statistical thermodynamics of the system.

The confining potential arises from non-bonding interactions between the H_2 molecule and the cage wall. In the case of $H_2@C_{60}$ the interactions are exclusively between hydrogen and carbon. The group of Bačić has pioneered the theoretical description of this cage potential leading to a refined evaluation of the energy levels that characterize the quantum dynamics of H_2 [21,22,23,24]. These computational investigations illuminate an important aspect of the dynamics, namely the coupling of translational and rotational angular momentum. This is mediated by the 5D-cage potential that has terms sensitive to the orientation of the axis of the H_2 molecule relative to the normal to the cage wall.

The first Letter detailing an INS investigation of a hydrogen endofullerene [16] dealt with a preliminary study of $H_2@ATOCF$ in which the H_2 molecules occupied an anisotropic cage potential. This was followed by a Communication [17] which concentrated on the isotope effects in the mixed isotope HD/H_2 system where the molecules occupied a closed cage. In this paper we present an in-depth investigation of the neutron scattering of hydrogen endofullerenes where the emphasis will be on $H_2@C_{60}$. A sufficiently large sample of this model system is available for the first time to enable the coupling between translational and rotational angular momentum (TR coupling) to be investigated. INS spectra have been recorded on different time-of-flight spectrometers under different instrument configurations covering a range of energy windows and resolutions. This has enabled the energy levels of the entrapped H_2 molecules to be determined with high accuracy from the INS transition energies. The TR coupling, which is found to raise degeneracies and lead to splittings of particular states, will be discussed in depth.

Some further INS results are also presented on the open cage endofullerene, $H_2@ATOCF$, which has an anisotropic cage potential. This is an interesting member of the endofullerene family because, in contrast to C_{60}, the cage has very low symmetry. This fully lifts the rotational and translational degeneracy and this study formally identifies the third translational mode by INS for the first time.

When a neutron is scattered by a nucleus, momentum is conserved as well as energy. The energy transfer enables the energy level structure to be elucidated but the momentum transfer, $\hbar\kappa$, also contains information on the confinement of the H_2 molecule. Therefore, momentum dependence spectra $S(\kappa)$ will also be interpreted to give insight into the scattering of neutrons by entrapped hydrogen. It will be

4

shown how this may be used as a diagnostic tool in the assignment of the INS transitions. New results on the mixed isotope sample $HD/H_2@C_{60}$ are presented addressing the κ-dependence of scattering from HD and contrasting it with the corresponding behavior of H_2.

2. Theory

2.1 Quantum translator-rotator energy levels

The dihydrogen molecule possesses rotational angular momentum which is quantized. The free H_2 molecule is a three dimensional rotor with rotational energy levels $E_{rot} = BJ(J+1)$ where $B = \hbar^2/2I_m$ is the rotational constant, I_m is the moment of inertia and $J = 0, 1, 2, \ldots$ is the rotational quantum number. The degeneracy of the J'th level is $g_r = 2J + 1$ with angular momentum sub-levels labeled by the quantum number $m_J = -J, -J+1, \ldots, +J$. Given the bond length of the free H_2 molecule is $d_{HH} = 0.74$Å, then $B = 7.37$meV.

The translation of the H_2 molecule is constrained by its physical confinement within the fullerene cage. For C_{60} the cage potential is almost isotropic with the minimum coinciding with the centre of the cage. Therefore the system is a practical realization of the 'particle in a potential well'. Making allowance for the dimensions of the H_2 molecule, the effective diameter of the potential well is approximately 0.8Å. The H_2 molecule has three translational degrees of freedom so its translational energy is characterized by three quantum numbers. Given the near isotropic symmetry, two of these represent the particle's translational angular momentum. Modeling the potential as a 3D isotropic harmonic oscillator we are led to define the principal quantum number $n = 0, 1, 2\ldots$ and the orbital angular momentum quantum number l where $l = n, n-2, \ldots, 1$ for odd n and $l = n, n-2, \ldots, 0$ for even n. The translational degeneracy is governed by the angular momentum states and in the absence of any coupling between rotation and translation this is $g_t = 2l + 1$. A third quantum number is therefore $m_l = -l, -l+1, \ldots, +l$ although in practice this is found not to be a good quantum number due to translation-rotation coupling. Translational energy is quantized and simple calculations show the energy splittings are of order 20 meV.

The two spin ½ nuclei of the dihydrogen molecule are identical fermions, therefore we identify two spin-isomers, o-H_2 with total nuclear spin $I = 1$ and p-H_2 with $I = 0$. The antisymmetry principle, being the most general form of the PEP, must apply in determining the allowed eigenstates. This results in an entanglement of space and

spin degrees of freedom such that the rotational states of p-H_2 have even $J = 0, 2, 4, \ldots$ while o-H_2 has odd $J = 1, 3, \ldots$. o-H_2 is metastable with respect to p-H_2. Ortho-para conversion between spin isomers is spin-restricted and can only be mediated by a magnetic interaction connecting space and spin. In the diamagnetic environment of C_{60} this means o-H_2 and p-H_2 remain as distinct species and ambient conversion times are extremely long.

The interaction with the fullerene cage wall has a component that depends upon the orientation of the H-H axis, so the potential depends upon the rotational eigenstate. This is the origin of the coupling between translational and rotational angular momentum. Xu *et al* [21] characterize the total angular momentum of the H_2 states, representing a vector sum of orbital and rotational angular momentum. Applying the usual rules we may characterize the translation-rotation states by the quantum number $\lambda = l + J, l + J - 1, \ldots, |l - J|$ and its projection along a quantization axis by the quantum number $m_\lambda = -\lambda, -\lambda + 1, \ldots, +\lambda$ so that the degeneracy is $g_\lambda = 2\lambda + 1$. The effect of the TR coupling is to raise the $2l + 1$ degeneracy of an eigenstate and the states are classified by the TR quantum number λ.

In Fig. 2 we present an energy level diagram for $H_2@C_{60}$ where the states are characterized by the quantum numbers J, n, l, λ. The energy levels have been determined for the ground vibrational state from the INS data reported in this paper, adapting the scheme reported by Xue *et al* [23] which was optimized for the IR spectrum of $H_2@C_{60}$ (therefore representing an excited vibrational state). States with common J are arranged in columns and within these the states are split first by the translational energy governed by the principal quantum number n. Second there is a smaller splitting arising from TR coupling which raises the $2l + 1$ degeneracy of states with quantum number l. Rotational energies separate the columns of spin isomers with common values of n, so that, for example, the ground states of p-H_2 $(J, n, l) = (0, 0, 0)$ and o-H_2 $(J, n, l) = (1, 0, 0)$ are separated in energy by $2B$.

Deviations from isotropic symmetry lead to further splittings, raising other degeneracies. One of these is unimportant to the lower lying states probed in this INS investigation and arises from the small deviation from spherical symmetry (icosahedral) of the C_{60} cage potential; this introduces a very small splitting of levels with $\lambda \geq 3$ [23]. More important to this study is the change in the energy level scheme when the cage potential is rendered anisotropic. This has the effect of quenching the orbital angular momentum, raising the degeneracy associated with the

quantum number l. In this case it is more appropriate to classify the translational states in terms of three Cartesian quantum numbers, n_x, n_y, n_z. Further, the anisotropic perturbation introduces a component into the potential that depends on the orientation of the molecule and splits the rotational levels, raising the $2J+1$ degeneracy.

2.2 Inelastic neutron scattering

2.2.1 H₂ molecule

Neutron scattering from molecular hydrogen enjoys particular interest because the two nuclei are indistinguishable quantum particles in close proximity. Therefore, spin correlations in the scattering process from the two-centre quantum object have a profound influence on the experimental observations. This was appreciated since the early days of neutron scattering and Elliott & Hartmann, [25] and Jones & Koppel [26] among others have given theoretical descriptions for scattering from H₂ in the gaseous and liquid phases. More recently, Yildirim and Harris [27] and Xu *et al* [28,29] have discussed the INS theory of entrapped H₂ where the translations are quantized.

Neutrons are scattered from a pair of ¹H nuclei. Defining the energies and wave vectors of the incident and scattered neutron by $E_i, \mathbf{k}_i$ and $E_f, \mathbf{k}_f$ respectively, we may write the neutron energy transfer as $\hbar\omega = E_i - E_f = \Delta E$ and neutron momentum transfer as $\hbar\boldsymbol{\kappa} = \hbar\mathbf{k}_i - \hbar\mathbf{k}_f$. The differential scattering cross section is, [25,26,27]

$$\frac{\partial^2 \sigma}{\partial\Omega\partial\omega} = \frac{k_f}{k_i} \sum_{i,f} p_i \left| \langle i|V|f \rangle \right|^2 \delta\left(\hbar\omega - E_i + E_f\right) \qquad (1)$$

where the matrix elements are those of the interaction potential,

$$V = \sum_{\alpha=1,2} e^{i\boldsymbol{\kappa}.\mathbf{R}_\alpha} \left\{ b_{coh} + \frac{b_{incoh}}{2} \boldsymbol{\sigma}.\mathbf{I}_\alpha \right\} \qquad (2)$$

so that the incoherent neutron scattering transitions are mediated by a scalar coupling between neutron spin, $\boldsymbol{\sigma}$, and the proton labeled $\alpha = 1,2$ with spin $\mathbf{I}_\alpha$ and position vector $\mathbf{R}_\alpha = \mathbf{R}_0 + (-1)^\alpha \boldsymbol{\rho}/2$. Here $\mathbf{R}_0$ is the vector defining the centre of mass of the molecule and $\boldsymbol{\rho}$ is the vector connecting the two protons. p_i is the

statistical weight of the initial state $\left|i\right\rangle=\left|\sigma_i\right\rangle\left|\psi_i\right\rangle$ of the compound neutron-H_2 system which is written as a product of neutron spin wavefunction $\left|\sigma_i\right\rangle$ and molecular wavefunction $\left|\psi_i\right\rangle$. Similarly, $\left|f\right\rangle$ is the final state wavefunction. b_{coh}, b_{incoh} are the coherent and incoherent scattering lengths of the hydrogen nucleus.

Evaluating the summation over the protons α, then for each molecule in the sample,

$$V_{HH}=e^{i\mathbf{\kappa}.\mathbf{R}_0}\left\{2b_{coh}\cos\left(\tfrac{1}{2}\mathbf{\kappa}.\mathbf{\rho}\right)+\frac{b_{incoh}}{2}\cos\left(\tfrac{1}{2}\mathbf{\kappa}.\mathbf{\rho}\right)\mathbf{\sigma}.\left(\mathbf{I}_1+\mathbf{I}_2\right)+i\frac{b_{incoh}}{2}\sin\left(\tfrac{1}{2}\mathbf{\kappa}.\mathbf{\rho}\right)\mathbf{\sigma}.\left(\mathbf{I}_1-\mathbf{I}_2\right)\right\}$$

(3)

The second term in $\cos\left(\tfrac{1}{2}\mathbf{\kappa}.\mathbf{\rho}\right)$ is scaled by b_{incoh} and drives transitions for which there is no net change in total nuclear spin $\left(\mathbf{I}_1+\mathbf{I}_2\right)$. This would be a pure translational transition of o-H_2 where there is no simultaneous change in rotational state. Significantly, since its total nuclear spin is zero, the analogous transition for p-H_2 is driven only by the first term that scales as b_{coh}. For ^{1}H, $b_{coh}\ll b_{incoh}$, so the pure translational peaks of p-H_2 are virtually absent from the neutron scattering spectrum. The third term in $\sin\left(\tfrac{1}{2}\mathbf{\kappa}.\mathbf{\rho}\right)$ has the capacity to drive changes in total nuclear spin and consequently gives rise to transitions that interchange o-H_2 and p-H_2; due to the spin-symmetry these necessarily involve changes in rotational state and can include simultaneous changes in translational state. This term also scales with b_{incoh} so it makes a significant contribution to the INS spectrum.

A detailed examination of the neutron scattering cross-section for entrapped H_2 requires evaluation of Eqn. (1) with Eqn. (3) and hence detailed knowledge of the molecular wavefunctions of o-H_2 and p-H_2. In a regime where T-R coupling is significant then only a numerical approach is viable, using numerical wavefunctions derived from a modeled cage potential. [29] This is beyond the scope of the present paper. However, it will be appropriate to consider an approximation in the limit where T-R coupling is negligible and the molecular wavefunctions are products of pure rotational and translational eigenfunctions. This will facilitate the interpretation of selected peaks in the experimental INS spectrum. Using this approximation Yildirim & Harris [27] have derived the scattering law from Eqn. (1) for the $J=0\rightarrow1$ transition converting p-H_2 to o-H_2 in their ground translational states. This may be written in the form,

$$S(\kappa,\omega)_{000\to100}^{p\to o} \propto \frac{k_f}{k_i} b_{incoh}^2 p_{000} e^{-\frac{1}{3}\kappa^2\langle u^2\rangle} \left(j_1\left(\kappa r_{HH}\right)\right)^2 \delta\left(\hbar\omega - E_{000} + E_{100}\right) \qquad (4)$$

where $j_n\left(\kappa r_{HH}\right)$ is a spherical Bessel function of order n, $r_{HH} = d_{HH}/2$ is the distance of the H-nucleus from the centre of mass of the molecule with inter-nuclear distance d_{HH}, and $\frac{1}{6}\kappa^2\langle u^2\rangle$ is the Debye-Waller factor where $\langle u^2\rangle$ is the mean squared displacement of the hydrogen molecule. This transition appears as a peak centered on $\hbar\omega = E_{100} - E_{000}$ in neutron energy (NE) loss since the final state $J=1$ of o-H_2 has higher energy than $J=0$ of p-H_2. The subscripts identify the states by their quantum numbers (J,n,l). A similar expression applies for the $J=1\to0$ peak in NE gain, differing only in numerical factors including statistical weight.

An approximation for the scattering law relating to the translational transition of o-H_2, $(100)\to(111)$, may also be derived from [27]; we find,

$$\begin{aligned}
S(\kappa,\omega)_{100\to111}^{o\to o} &\propto \frac{k_f}{k_i} b_{incoh}^2 p_{100} e^{-\frac{1}{3}\kappa^2\langle u^2\rangle} \kappa^2\langle u^2\rangle \\
&\times \left\{\left(j_0\left(\kappa r_{HH}\right)\right)^2 + 2\left(j_2\left(\kappa r_{HH}\right)\right)^2\right\}\delta\left(\hbar\omega - E_{100} + E_{111}\right)
\end{aligned} \qquad (5)$$

The term in κ^2 is characteristic of translational transitions and arises from a displacement operator associated with the expansion of $e^{i\kappa.\mathbf{R}_0}$. Therefore, comparing Eqns. (4) and (5) we expect the dependence of the spectrum on momentum transfer $\hbar\kappa$ to facilitate the spectral assignment to different modes.

2.2.2 HD molecule

For the HD molecule there is no spin symmetry since the two nuclei are of different species. This means the spin correlations that characterize the neutron scattering expressions for H_2 no longer apply. Furthermore, the incoherent scattering cross section of ^2H is only 2.5% that of ^1H so the spectrum is dominated by scattering from ^1H and in determining the scattering law we may approximate the HD molecule as a single nuclear particle with effective spin ½. We may simply write,

$$V_{HD} = e^{i\kappa.\mathbf{R}_0} e^{i2\kappa.\boldsymbol{\rho}/3}\left\{b_{coh} + b_{incoh}\boldsymbol{\sigma}.\mathbf{I}\right\} \qquad (6)$$

where the proton is now $2|\boldsymbol{\rho}|/3$ from the centre of mass. It is evident from Eqn. (6) that unlike H_2, all rotational and translational transitions of HD contribute to the INS spectrum with significant intensity.

3. Experimental details

INS spectra were recorded on two time-of-flight spectrometers at the Institut Laue-Langevin (ILL), Grenoble. IN4C is a high flux medium resolution spectrometer situated on a thermal neutron beam. [30] The wavelength of the incident neutron beam is selected in the range $1.1 \le \lambda_n \le 1.8\,\text{Å}$ using Bragg diffraction from a curved highly ordered pyrolytic graphite monochromator. A Fermi-chopper provides the pulsed neutron structure, with scattered neutron energy analysis being determined by time-of-flight across a 2m flight chamber. Spectra in NE loss and gain are accessible with the energy range determined by the incident neutron wavelength. The spectral resolution and the accessible Q-range are also dependent on incident wavelength so a variety of set ups were used, optimizing the information content of the recorded spectra.

IN5 is a disk-chopper time-of-flight spectrometer operating on a cold neutron beam line at the ILL. [30] The incident neutron wavelength is selected in the range $1.8 \le \lambda_n \le 20\,\text{Å}$ by setting the rotation rate and phase of six pairs of counter-rotating choppers. The scattered neutron energy analysis is determined by time-of-flight across a 4m flight chamber. The array of pixilated position sensitive detectors occupies a large surface area (30m^2) so the sensitivity benefits from the large solid angle over which neutrons were collected. For the purposes of this investigation, the IN5 spectrometer was set up to provide optimum spectral resolution in NE gain.

The endofullerene sample synthesis was conducted using published procedures [1,2] (see supplemental material). The powdered samples were encapsulated within thin rectangular aluminum foil packages and mounted on a sample stick inside a helium cryostat providing stable temperatures in the range $1.2 \le T \le 300K$. Samples masses were as follows: $H_2@C_{60}$, 250 mg; $HD/H_2@C_{60}$, 190 mg; $H_2@ATOCF$ 492 mg. Hydrogen loading of the cages was very close to 100%. For $H_2@C_{60}$, scattering from the C_{60} cage is generally weak: librations appear at low energy transfer, $\Delta E < 5$ meV, and cage vibrations at discrete frequencies above 30meV, for example 33.6meV and 42meV. Where appropriate the cage component was removed from the spectrum by weighted subtraction of the scattering recorded on a 1g empty cage sample of C_{60}. For $H_2@ATOCF$ the scattering from the hydrogenous sidegroups that stabilize the

cavity orifice was subtracted using a spectrum recorded on a sample of ATOCF that had no H_2 loaded.

The energy transfers characterizing peaks in the INS spectrum were determined by fitting Gaussian functions which are a good representation of the instrument resolution. The width of the resolution function (Full Width at Half Maximum: FWHM) depends on the spectrometer configuration and is also a function of energy transfer.

4. Results

4.1 Rotations and translations of H_2@C_{60}: isotropic cage symmetry

The low temperature IN4C spectrum (1.6K) recorded with incident neutron wavelength $\lambda_n = 1.6\,\text{Å}$ is shown in Fig. 3. The peak centered on 14.69 ± 0.05 meV in NE loss is the principle rotational line, arising from the transition $(J,n,l) = (0,0,0) \rightarrow (1,0,0)$ that inter-converts p-H_2 and o-H_2 in their ground states.

This defines the rotational constant since the transition is characterized by the energy splitting $2B$. Within experimental uncertainties this value agrees with the value of B calculated for free H_2 so we can infer the physical structure of the molecule is largely unaffected by its incarceration inside the cage.

The same transition in the reverse direction gives rise to the peak in NE gain at -14.71 ± 0.05 meV. The observation of this peak with finite intensity mirrors earlier INS investigations [16,17], where, arising from the spin-restricted nature of the transition, o-H_2 and p-H_2 are unable to interconvert in response to changes in temperature and the populations of the two spin isomers are frozen in when the sample is cooled.

The rotational peaks in Fig. 3 have widths equal to the instrument resolution and are fitted well by a Gaussian line shape function. The different observed line widths in NE loss (FWHM: 1.1meV) and gain (FWHM: 2.3meV) reflects the variation of the IN4C spectrometer resolution with energy transfer.

In Fig. 4 the intensity of the 14.7 meV rotational peak is plotted as a function of momentum transfer $S(\kappa)$ for (a) NE gain and (b) NE loss peaks. To access a broad range of κ, these data have been recorded with incident neutron wavelength $\lambda_n = 1.1\,\text{Å}$. The shape of $S(\kappa)$ is the same for both NE gain and loss peaks, showing a maximum at approximately $\kappa = 3.9\,\text{Å}^{-1}$. The solid lines are fits with the function $S(\kappa) = Ae^{-\frac{1}{3}\kappa^2\langle u^2\rangle}\left(j_1\left(\kappa r_{HH}\right)\right)^2$ (Eqn. (4)) containing two adjustable parameters,

namely an amplitude A and $\langle u^2 \rangle$. The fits display very good correspondence with the data, confirming the assignment. The best fit parameters are $\langle u^2 \rangle = 0.126 \pm 0.002$ Å^2 (NE loss) and $\langle u^2 \rangle = 0.122 \pm 0.002$ Å^2 (NE gain).

The peak centered on approximately 22.5meV is assigned to the first translational transition of o-H$_2$, $(1,0,0) \rightarrow (1,1,1)$. This peak displays systematic deviation from a Gaussian line shape indicating the presence of structure that is not fully resolved; we shall return to this aspect in the next section. Firstly, however we shall address the dependence of this feature on momentum transfer which is plotted in Fig. 4c. The solid line is the fit with the function

$$S(\kappa) = A e^{-\frac{1}{3}\kappa^2 \langle u^2 \rangle} \kappa^2 \langle u^2 \rangle \left\{ \left(j_0 (\kappa r_{HH}) \right)^2 + 2 \left(j_2 (\kappa r_{HH}) \right)^2 \right\},$$ Eqn. (5). Apart from the

amplitude which has arbitrary instrument dependent units, there is just one fitting parameter with best fit value $\langle u^2 \rangle = 0.102 \pm 0.002$ Å^2. Superficially the $S(\kappa)$ curve has similar shape to that of the rotational line with the maximum occurring at a similar value of κ. However there are significant systematic differences, in particular with a longer 'tail' for the translational data at high κ. The quality of the fit confirms the assignment of the translational peak, and the energy transfer conforms well with the energy level scheme devised by Xu *et al* [23] based on IR spectroscopy.

4.2 Fine structure arising from TR coupling in H$_2$@C$_{60}$

In Fig. 5 the translational peak of o-H$_2$ recorded with incident wavelength $\lambda_n = 1.6$ Å is presented with a larger energy scale. The degeneracy of the (111) state is 3 so it is expected this spectral feature will be a triplet of λ-sublevels split by TR coupling. Indeed, the observed peak fits poorly to a single Gaussian indicating the presence of fine-structure. Accordingly the feature has been fitted to a triplet of Gaussians with widths constrained to conform to the known resolution function of IN4C (FWHM: 1.1 meV) in this configuration. The solid lines in Fig. 5 show the best fit components. A pair of peaks with energy transfer 22.17 ± 0.05 meV and 22.88 ± 0.05 meV have similar amplitude but a third peak appears as a shoulder at 24.3 ± 0.1 meV with much lower amplitude. This structure in the translational peak provides compelling experimental evidence for TR coupling with magnitude of order 1 meV. We shall assign the temporary labels $\lambda^{(a)}, \lambda^{(b)}, \lambda^{(c)}$ signifying in ascending energy the three members of the (111) triplet, Fig. 2. The splitting of the three is unequal so that the

splitting $\lambda^{(c)} - \lambda^{(b)}$ is 2.0 times $\lambda^{(b)} - \lambda^{(a)}$. This splitting scheme conforms well in magnitude with the calculations of Xu *et al* [23] based on a model potential for the cage.

4.3 Translation-rotation transition in H₂@C₆₀

The scattering law has the statistical weight of the initial state as a factor, therefore it is clear that all observed peaks in a low temperature spectrum must originate in the ground state of either p-H$_2$ (000) or o-H$_2$ (100). Applying this principle, a definitive assignment is made of the peak at 8.08 ± 0.03 meV to $(100) \rightarrow (011)$, namely the transition from o-H$_2$ in the ground state to p-H$_2$ in the first excited translational state. This involves simultaneous changes in rotational and translational state. It is an interesting feature because, knowing the measured translational energy, we are able to infer (Fig. 2) that the first translational splitting of p-H$_2$ is 22.78 ± 0.06 meV. Since p-H$_2$ has no rotational angular momentum and therefore experiences no splitting due to TR coupling, this provides our best measure for the quantization of translational energy. Furthermore, it is notable this value approximates well the energy transfer of the central member of the (111) triplet of o-H$_2$ (Fig. 5 and section 4.2 above). However, due to the strongly asymmetric amplitudes of the $(100) \rightarrow (111)$ triplet, it is significant that the unperturbed translational energy does not coincide with the centre of gravity of the observed band. Therefore, it is clear that the most accurate values of translational and rotational splittings will only be obtained when all members of a multiplet are fully resolved in the spectrum.

4.4 Higher order transitions in H₂@C₆₀

To gain access to higher energy transfers, the 1.6K IN4C spectra were recorded with shorter incident neutron wavelengths of $\lambda_n = 1.2$ Å and $\lambda_n = 1.1$ Å, see Fig. 6. These spectra are characterized by a broader spectrometer resolution function so not all spectral features may be resolved. Discrete bands are observed up to the highest accessed energy transfer, 60meV.

Being close in energy transfer to $4B$, the peak centered at 29.2 ± 0.2 meV is assigned to the pure rotational transition $(100) \rightarrow (200)$. Within the range of experimental uncertainties this energy transfer is twice that of the principal rotational peak, as expected for a free rotor.

The band at 37.8 ± 0.1 meV coincides closely with the energy of the (111) triplet of o-H_2 and therefore can be assigned to $(000) \rightarrow (111)$, namely the transition from the ground state of p-H_2 to the first excited translational state of o-H_2. Analogous to the 8.08 meV peak, this involves simultaneous changes in rotational and translational state. The structure of the triplet, which is known from the lower energy translational peak, is unresolved in this band at this resolution. However, the fit with a single Gaussian line shape coincides well with the average of the lowest and highest energies of the triplet, suggesting these two components may have similar INS amplitudes in this band.

The band centered on 46.6 ± 0.1 meV has energy slightly larger than twice the unperturbed translational splitting and consequently may be assigned to a translational transition of o-H_2, namely $(100) \rightarrow (12l)$. The $n = 2$ state has two possible translational angular momentum values $l = 0, 2$ which become non-degenerate in the presence of an anharmonic cage potential. [21,22,23] According to the calculations of Xu *et al*, [23] the $l = 2$ state has the lowest energy and the $l = 0$ lies approximately 5 meV higher. The 46.6 meV band is only marginally broader than the resolution function with FWHM of 2.5 meV in the $\lambda = 1.2$ Å spectrum and is assigned to $(100) \rightarrow (122)$. There are some small systematic deviations from the Gaussian fitting function particularly on the low energy side of this band so, given the TR quantum number λ can be 3, 2 or 1 for the (122) state, there may be some unresolved structure due to TR coupling. However, the band is insufficiently resolved to permit a free fit and independent knowledge of the relative INS intensities would be required to extract TR coupling parameters for this band.

The $(100) \rightarrow (120)$ transition either has very small intensity and/or it is split from the (122) state by approximately 5 meV in which case it will overlap the remaining band observed at 51.8 meV. Therefore, we are currently unable to assign the energy of the (120) state.

Given the unperturbed translational splitting of 22.78 meV and the measured energy of the (200) state (44.0 meV), the first excited translational state (211) of p-H_2 is expected to have an energy of approximately 66.8 meV. The 51.8 ± 0.2 meV band observed in the $\lambda_n = 1.1$ Å spectrum therefore coincides closely with the $(100) \rightarrow (211)$ transition, to which it is assigned. The (211) band has three possible values of $\lambda = 3, 2, 1$ which will be split by TR coupling. This band is resolution limited

in the $\lambda_n = 1.1\,\text{Å}$ spectrum (FWHM 3.3 meV) so any such TR structure within this triplet lies within the linewidth. This is in broad agreement with the calculations of Xu *et al* who calculate TR splittings no larger than 1.4 meV for this band [23].

Inspecting the energy level scheme, the only transition that has not been assigned within the energy transfer range probed, is $(100) \rightarrow (02l); l = 0, 2$. Given the $(nl) = (22)$ translational state of o-H_2 is observed to lie 46.6 meV above its ground state, we can infer the $(100) \rightarrow (022)$ band will lie at approximately 31.9 meV. A small shoulder is indeed observed at 32.0 ± 0.3 meV in the $\lambda_n = 1.2\,\text{Å}$ spectrum and we assign this feature to this band. (Note: A C_{60} vibrational mode lies at 33.6 meV but this has been subtracted in the empty cage subtraction and is well separated from the mode assigned to $H_2@C_{60}$). We are unable to discern evidence in the 1.6K INS spectrum for the related $(100) \rightarrow (020)$ transition which Xu *et al* [23] predict lies approximately 3 meV higher in energy than $l = 2$, so it may have small intensity.

4.5 Temperature dependence studies of $H_2@C_{60}$

The scattering cross-section depends linearly on the statistical weight of the initial state, p_i, that characterizes a transition, Eq. (1). Therefore, with increasing temperature excited states become populated and new peaks appear in the INS spectrum. Some of these appear in NE gain, being the 'emission' partners of transitions previously observed in NE loss at low temperature. However, other transitions are observed to be new and may be used to refine our knowledge of the energies of the $H_2@C_{60}$ states. Temperature dependence measurements were conducted on the IN5 spectrometer with an incident wavelength $\lambda_n = 5\,\text{Å}$. This configuration provides the NE gain spectrum and a resolution of ≈0.5 meV (FWHM) in the region of the main rotational line, $J = 1 \rightarrow 0$.

In Fig. 7 the IN5 spectrum of $H_2@C_{60}$ is shown, recorded at three temperatures, 1.5K, 120K and 240K. At 1.5K only the $J = 1 \rightarrow 0$ rotational line is present. Consider the energy transfer region $-20 \leq \Delta E \leq -5$ meV : with increasing temperature we first note the appearance of a strong band at -14.1 ± 0.1 meV. This is assigned to the transition between $\lambda^{(a)}$ of the (111) triplet of o-H_2 and the (011) singlet of p-H_2, coinciding precisely in energy with our previous evaluation of the energies of these states. This is a transition between the first excited translational states of $J = 1$ and $J = 0$, see Fig. 2. The related transition of this triplet originating in $\lambda^{(b)}$ cannot be

resolved, being superimposed on the $J = 1 \rightarrow 0$ rotational line. Furthermore, the transition originating in $\lambda^{(c)}$ of the (111) triplet would be expected in the region -16 meV. A small feature appears there at higher temperature which may be this transition but it must have low intensity, in agreement with NE loss.

Plotting the normalized amplitudes of the -14.1 and -14.70 meV lines in NE gain in Fig. 8 supports their assignment. The amplitude of the -14.70 peak diminishes with increasing temperature as excited states of o-H_2 are populated, while the amplitude of the -14.1 meV peak increases. Adopting the scheme of Xu *et al* [23] we may assign $\lambda^{(a)} = 1$, $\lambda^{(b)} = 2$ and $\lambda^{(c)} = 0$ and hence use the associated degeneracies in an evaluation of the statistical weights p_i of these states. The latter, calculated assuming Boltzmann statistics, are represented by the solid lines in Fig. 8. General agreement with the observed transition amplitudes is observed, even in the absence of any modeling of the relative transition matrix elements. Note in particular the observed amplitude of the -14.70 meV peak lies higher than the calculated Boltzmann weighting of the $J = 1 \rightarrow 0$ line. However the $\lambda^{(b)} = 2$ member of the triplet is superimposed on this peak and should be incorporated in a calculation of the total amplitude. We do not currently have *a-priori* knowledge of the transition matrix elements but using the transition matrix element ratio $\left| V_{\lambda^{(b)}} \right|^2 / \left| V_{\lambda^{(a)}} \right|^2 \simeq 0.4$ we obtain a good overall fit to the amplitude shown with the dashed line in Fig. 8. Furthermore the figure shows the small amplitude of the peak originating in $\lambda^{(c)} = 0$ at approximately 16.2 meV is at least partly explained by the low degeneracy of this state and its influence on the statistical weight.

In the energy transfer region $-10 \leq \Delta E \leq -4$ meV, the IN5 spectra have a resolution (FWHM) of order 0.5 meV. Potentially this high resolution enables the energy levels and any splittings arising from TR coupling to be identified and accurately determined. An example of this is provided by the appearance of small peaks in the region of low energy transfer when the temperature is raised to 240K, see Fig. 7. These peaks are shown more clearly in Fig. 7b where a quasi-elastic baseline, modeled as a polynomial, has been subtracted. These narrow peaks have been assigned on the basis of the energy level diagram determined at low temperature, but given they are recorded with high resolution they have enabled a refinement of those energies. The peak at -8.11 ± 0.05 meV is the NE gain partner of the $(100) \rightarrow (011)$ peak assigned in the low temperature IN4C spectrum. However, there are small features at -7.16 ± 0.05 and -6.40 ± 0.05 meV which may be assigned to

16

the transition $(200) \rightarrow (111)$, identifying the $\lambda^{(a)}$ and $\lambda^{(b)}$ members of the (111) triplet respectively.

Similarly, the peaks at -10.25 ± 0.05 meV and -9.53 ± 0.03 meV are two members of the $(022) \rightarrow (111)$ triplet, arising from the transition to the $\lambda^{(a)}$ and $\lambda^{(b)}$ final states respectively. These peaks enable the energy of the (022) state to be refined to 47.1 ± 0.2 meV. The other member of this triplet, arising from the transition to $\lambda^{(c)}$, would appear at -8.1 meV which overlaps with a stronger band and hence cannot be independently identified.

Anharmonicity is responsible for splitting the $l = 0, 2$ states of $(Jnl) = (02l)$. The peaks with energy transfers -11.87 ± 0.05 meV and -10.6 ± 0.1 meV enable us to identify the energy of the (020) state for the first time in this study. These peaks have an energy difference which is consistent with the splitting of the $\lambda^{(b)}$ and $\lambda^{(c)}$ members of the (111) triplet, therefore identifying the peaks in question as two members of the $(020) \rightarrow (111)$ transition so that $E_{020} = 49.5 \pm 0.2$ meV. The third member of this band with final state $(111\,\lambda^{(a)})$ would be expected to appear at 12.60 meV but does not appear with high intensity in the spectrum. This assignment of the (020) energy suggests the splitting arising from anharmonicity is $E_{022} - E_{020} = 2.4$ meV. This compares with the calculation of 3.28 meV by Xu $et\ al$ [23]. The assignment $E_{020} = 49.5 \pm 0.2$ meV currently provides the best match to the INS spectrum, but calculations of the transition matrix elements are required to confirm this through comparison of the theoretical and experimental peak intensities.

At energy transfers $|\Delta E| > 20\ \mathrm{meV}$ in the IN5 spectrum of Fig. 7, many features identified in the NE loss spectrum begin to appear with increasing temperature, but they are augmented by additional peaks involving excited states. This results in many overlapping lines. An initial examination of the line intensities shows they are broadly consistent with Boltzmann statistics but a detailed analysis of this region will be undertaken in a future paper.

4.5 HD@C$_{60}$: isotope effects

The INS spectrum of the isotopic mixture of HD@C$_{60}$ and H$_2$@C$_{60}$ has been discussed in an earlier paper. [17] With the acquisition of the pure H$_2$@C$_{60}$ we are in a position to determine the difference spectrum and hence to confirm the assignments to the HD species. In Fig. 9 the spectrum of HD@C$_{60}$ is presented, recorded at 1.8K with $\lambda_n = 1.65\ \mathrm{\mathring{A}}$. Since the mixed isotope and pure H$_2$@C$_{60}$ experiments were conducted

at different times, there are small differences in spectrometer configuration which give rise to imperfect subtraction, however the quality of the difference spectrum is sufficiently good to enable the essential features to be interpreted. The low temperature spectrum has two peaks confirming their assignment to the $J = 0 \rightarrow 1$ rotational line (10.0 ± 0.1 meV) and the $J = 0; n = 0 \rightarrow 1$ translational line (19.1 ± 0.1 meV). Significant is the absence of the rotational line in NE gain highlighting the absence of spin-isomers for HD, so that species with odd and even J all equilibrate.

The κ-dependence of the rotational and translational lines of HD@C_{60} is presented in Fig. 10. The maxima of the rotational and translational curves for HD appear at $\kappa =$ 3.9 and 3.2 $\mathring{A}^{-1}$ respectively. This is different to the behavior of H_2@C_{60} where these maxima appear at approximately the same value of κ. This observation will be addressed in Section 5.

4.6 H_2@ATOCF: anisotropic cage

The first INS investigation on the open cage hydrogen endofullerene H_2@ATOCF was reported in an earlier paper [16] and the group of Bačić has applied their computational methodology developed on H_2@C_{60} to calculate the potential energy surface and the H_2 energy levels. [31] Significantly, the anisotropy of the cage potential raises the rotational and translational degeneracy. Due to the lack of symmetry the translational angular momentum is quenched and the translational eigenstates are more properly classified by three Cartesian quantum numbers. The three sub-levels, $m_J = 0, \pm 1$, associated with the $J = 1$ ground state of o-H_2 were resolved in the INS experiment on IN4C [16] but only two of the three translational modes at 17.07 and 17.91 meV were identified in the first spectrum with incident neutron wavelength $\lambda_n = 1.8 \mathring{A}$ and with energy transfer $\Delta E \le 20$ meV. These are pure translational transitions converting the ground and first excited translational states of $J = 1$, o-H_2.

An INS spectrum of H_2@ATOCF recorded with $\lambda_n = 1.24 \mathring{A}$ and energy transfer range $\Delta E \le 45$ meV is presented in Fig. 11 ($T = 2.5$ K). This is a difference spectrum, following subtraction of the scattering of the empty ATOCF cage. The inset shows the $\lambda_n = 1.8 \mathring{A}$ spectrum. The resolution of the $\lambda_n = 1.24 \mathring{A}$ spectrum is approximately 2.5 meV (FWHM) which is more than twice the resolution at $\lambda_n = 1.8 \mathring{A}$, so the rotational and translational splittings are unresolved in the shorter wavelength spectrum. The INS spectrum has no discernable narrow features between 20 and 28 meV (or below

10meV; not shown) but a group of lines appear in the range $28 \leq \Delta E \leq 42$ meV. These have been fitted with four Gaussians with best fit energy transfers of 30.2, 32.4, 34.9 and 38.6 ± 0.1 meV. In ref [16] it was estimated from the relative cage dimensions that the third translational mode would lie towards the lower end of this range. The momentum transfer dependence $S(\kappa)$ may be used to determine the assignment. In Fig. 12 the $S(\kappa)$ spectra are plotted for the peaks centered on 17.5 meV and 30.2 meV. The two curves have similar shape displaying maxima at $3.6\mathring{A}^{-1}$ suggesting they arise from similar types of transition. These are fitted with Eq. (5) showing good agreement with the translational function; best fit value $\langle u^2 \rangle = 108 \pm$ 0.004 $\mathring{A}^2$. Similar $S(\kappa)$ curves for the higher energy peaks in the range $32 \leq \Delta E \leq 41$ meV have maxima in the region $\kappa \simeq 5.2$ $\mathring{A}^{-1}$, much higher than for the 17.5 and 30.2 meV peaks, suggesting that higher order Bessel functions would be required to fit. Therefore, on the basis of their κ-dependence these higher energy peaks can be eliminated as candidates and an assignment of the third translational mode of H$_2$@ATOCF to the peak at 30.2 meV is confirmed. It is expected that the region $\Delta E \geq 32$ meV will contain higher order translational and rotational transitions, although the spectrometer resolution is currently unable to resolve the fine structure that is likely to characterize these peaks.

5. Discussion

All feasible transitions originating in the ground states of o-H$_2$ and p-H$_2$ have been observed and assigned in the low temperature INS spectrum of H$_2$@C$_{60}$ below 60 meV, providing a comprehensive and quantitative picture of the low lying energy levels. At high temperature the appearance of additional peaks originating in excited states augments our understanding of this energy level structure. The energy transfers of the observed INS transitions are collated in Table 1 and from these the energy levels of H$_2$@C$_{60}$ below 70 meV have been determined and are presented in Table 2 and Fig. 2. The magnitudes of the rotational and translational splittings revealed in this data are found to be consistent with the known physical properties of the C$_{60}$ cage and the hydrogen molecule, in accordance with discussions in earlier papers. [16,17,18]

It is striking that the majority of transitions observed in the INS spectrum of H$_2$@C$_{60}$ involve conversion between o-H$_2$ and p-H$_2$ species. These are driven by the third term in $\sin\left(\frac{1}{2}\boldsymbol{\kappa}.\boldsymbol{\rho}\right)$ in Eqn. (3). Analogous transitions are strictly spin-forbidden to

electromagnetic spectroscopies. Incoherent INS transitions that involve no change in spin-isomer are confined to pure translations of o-H_2, being driven by the second term in $\cos\left(\frac{1}{2}\boldsymbol{\kappa}.\boldsymbol{\rho}\right)$ in Eqn. (3); only two such peaks are observed in the energy transfer range studied. Both of these classes of transition scale with b_{incoh} so the intensities are expected to have generally similar magnitudes, as observed experimentally.

Significant to this investigation is the direct observation of TR coupling. The clearest example presented here is the splitting of the (111) triplet which is observed in a number of INS peaks. Analytically, an obvious first model entails scalar coupling between the rotational and translational angular momentum. In this case it is easily determined that the splitting of a TR multiplet is determined by $\Delta\varepsilon = a_{TR}\left(\lambda(\lambda+1)-J(J+1)-l(l+1)\right)$ where a_{TR} is a coupling constant. This raises the degeneracy and in accordance with observation leads to a splitting pattern of the three components that scales 1:2 in energy. However, assigning the TR quantum number λ-values on the basis of this scalar coupling model does not conform to the calculated energy level structure of Xu *et al* [23]. In their scheme, which is robustly assigned on the basis of the degeneracies exhibited by the calculated states, the values are assigned as $\lambda_a = 1$, $\lambda_b = 2$ and $\lambda_c = 0$. Therefore we conclude that the detailed properties of the 5-dimensional cage potential must contribute to the TR splitting patterns in combination with angular momentum coupling.

The peak amplitude of the λ_c component of the $(100)\rightarrow(111)$ translational triplet is much smaller than its two companions. Indeed this peak can only be detected in spectra recorded with high quality counting statistics and low background, explaining an ambiguity flagged in the earlier INS investigation of mixed isotope H_2/HD@C_{60}. [17] TR coupling is intimately implicated in this INS feature so to explain these amplitudes any theoretical analysis of the transition matrix elements must be based on numerical TR coupled eigenfunctions. This is a tractable proposition [29] but beyond the scope of the present paper.

Due to the absence of spin correlations for HD, sine and cosine terms in the interaction potential, Eqns. (2), (3) and (6), contribute equally to the INS spectrum of HD@C_{60}. This significantly influences the analytical expression describing the momentum transfer dependence of the inelastic neutron scattering, $S(\kappa)$. We can therefore infer from Yildirim and Harris [27] that for the rotational peak of HD, $S(\kappa)$

will contain both first and second order spherical Bessel functions. By contrast, the corresponding transition for H_2 is characterized by only a first order Bessel function, see Eqn. (4). We may write the following approximate expression for HD;

$$S\left(\kappa,\omega\right)^{(HD)}_{000\rightarrow100} \propto \frac{k_f}{k_i} b^2_{incoh} p_{000} e^{-\frac{1}{3}\kappa^2\langle u^2\rangle} \times$$

$$\left\{\left(j_1\left(\kappa r_{HD}\right)\right)^2 + \left(j_2\left(\kappa r_{HD}\right)\right)^2\right\}\delta\left(\hbar\omega - E_{000} + E_{100}\right) \tag{7}$$

where $r_{HD} = 2d_{HD}/3 = 0.493\times10^{-10}$ m is the distance of the H-atom from the centre of mass which does not coincide with the centre of the bond. The best fit to this function is shown with a solid line in Fig. 10 and conforms well with experiment in the measured range of κ. The best fit gives $\langle u^2\rangle = 0.900 \pm 0.006$ Å^2 which is 26% smaller than the corresponding parameter reported for H_2 in section 4.1. When H_2 is replaced by HD in a harmonic potential, simple calculations show a reduction in $\langle u^2\rangle$ of order 22% is expected so the observation is consistent with the theoretical behavior within experimental uncertainties and given the assumptions in deriving the theoretical behavior.

For the translational peak of HD, $S\left(\kappa\right)$ has some significant differences compared with H_2. At low temperature the translational transition in HD is predominantly between states with $J=0$ whereas for H_2 it is between states with $J=1$. The relevant expressions are not explicitly calculated by Yildirim and Harris [27] and the analytical form is currently unavailable. However, it is evident that leading terms in the $S\left(\kappa\right)$ expression for HD will contain zero'th and first order spherical Bessel functions. Assuming the following approximation,

$$S\left(\kappa,\omega\right)^{(HD)}_{000\rightarrow011} \simeq \frac{k_f}{k_i} b^2_{incoh} p_{000} e^{-\frac{1}{3}\kappa^2\langle u^2_{HD}\rangle}\kappa^2\langle u^2_{HD}\rangle$$

$$\times\left\{a\left(j_0\left(\kappa r_{HD}\right)\right)^2 + (1-a)\left(j_1\left(\kappa r_{HD}\right)\right)^2\right\}\delta\left(\hbar\omega - E_{000} + E_{011}\right) \tag{8}$$

and setting $\langle u^2_{HD}\rangle = 0.90$ Å^2 as above, the best fit has been evaluated. This provides a satisfactory representation of the experimental data: solid line Fig. 10. The relative weight of the two Bessel functions is determined by the best fit parameter $a = 0.61\pm0.05$.

6. Concluding Remarks

An analysis of the INS spectra of $H_2@C_{60}$ has enabled an accurate determination of the low-lying translation-rotation levels of molecular hydrogen inside its fullerene cage. The assignments are consistent with the TR coupling scheme developed by the group of Bačić [21,22,23] and the cage potential they calculated is shown to be a good approximation. As a model system for a quantum rotor trapped inside a 3D potential, the energy level scheme for $H_2@C_{60}$ measured by INS will be invaluable to future theoretical and experimental investigations of quantum motion, also enabling further refinements of non-bonding intermolecular potentials.

This INS study probes endohedral molecules in their ground vibrational state whereas infra-red experiments on the same endofullerene involve an excited vibrational state. [13,14] Making systematic allowance for the decrease in rotational constant with increasing vibrational quantum number, we find the energy level scheme measured by INS is in good agreement with that determined using infra-red spectroscopy.

The INS intensities of the three TR components of the first translational peak, $(J,n,l) = (100) \rightarrow (111)$, Fig 5, are strongly asymmetric. The $\lambda = 0$ component has much weaker intensity than the $\lambda = 1$ and $\lambda = 2$ components. Potentially, the relative INS intensities can provide further insight into the translation-rotation wavefunctions and their role in determining the matrix elements of the interaction potential, Eqns. (1) & (2). Analytical wavefunctions have not been derived, however numerical wavefunctions may be obtained using the approach of Bačić and co-workers [21,22,23]. The same group has recently formalised the numerical calculation of the inelastic neutron scattering law [29] so an interpretation of the relative INS intensities is a viable proposition in the near future.

Using the IN5 spectrometer, the appearance at high temperature of the narrow NE gain peaks in the range $-10 \leq \Delta E \leq -4$ meV has enabled the TR structure in the (111) triplet to be fully resolved, as highlighted in Fig. 7b. This provides further confirmation of the TR coupling scheme that was first assigned on the basis of the $(100) \rightarrow (111)$ transition observed with IN4C in NE loss.

The theoretical expressions reported here for the κ-dependence of the INS peak intensity have been derived under the assumption that TR coupling is zero and that rotational and translational coordinates are separable. Nevertheless, good agreement is obtained with experiment that provides physical and quantitative insight.

Significantly, we find that the κ-dependence provides a valuable diagnostic tool for distinguishing between rotational and translational INS peaks.

Acknowledgments

Table 1: $H_2@C_{60}$ observed INS transitions. [*]Indicates band centre of an unresolved multiplet

Initial state ($J\,n\,l\ \lambda$)	Final state ($J\,n\,l\ \lambda$)	Energy transfer / meV
000 0	100 0	14.69 ± 0.05
100 0	011 1	8.08 ± 0.03
100 0	200 0	29.2 ± 0.2
100 0	111 1	22.17 ± 0.05
100 0	111 2	22.88 ± 0.05
100 0	111 0	24.3 ± 0.1
000 0	111 0,1,2	37.8 ± 0.1 [*]
100 0	122 1,2,3	46.6 ± 0.1 [*]
100 0	211 1,2,3	51.8 ± 0.2 [*]
200 0	111 2	-6.40 ± 0.05
200 0	111 1	-7.16 ± 0.05
022 2	111 2	-9.53 ± 0.03
022 2	111 1	-10.25 ± 0.05
020 0	111 1	-10.6 ± 0.1
020 0	111 2	-11.87 ± 0.05
111 1	011 1	-14.1 ± 0.1
100 0	000 0	-14.71 ± 0.05

Table 2: H_2@C_{60}: energy levels determined by INS. *Indicates band centre: TR structure unresolved in spectrum. ‡Assignment of TR quantum numbers λ according to Xu *et al* [23].

J	n	l	λ	Energy / meV
0	0	0	0	0.0
1	0	0	0	14.70 ± 0.03
0	1	1	1	22.78 ± 0.05
1	1	1	$\lambda^{(a)} = 1$ ‡	36.87 ± 0.07
1	1	1	$\lambda^{(b)} = 2$ ‡	37.58 ± 0.07
1	1	1	$\lambda^{(c)} = 0$ ‡	39.0 ± 0.1
2	0	0	2	44.0 ± 0.1
0	2	2	2	47.1 ± 0.2
0	2	0	0	49.5 ± 0.2
1	2	2	3,2,1	61.3 ± 0.1*
2	1	1	3,2,1	66.5 ± 0.1*

Figure Legends

Fig. 1 The hydrogen endofullerenes $H_2@C_{60}$, $HD@C_{60}$ and $H_2@ATOCF$. (ATOCF: azacyclic-thiacyclic open-cage fullerene).

Fig. 2 The energy levels of molecular hydrogen in $H_2@C_{60}$ determined by inelastic neutron scattering. The states are labeled by their quantum numbers (Jnl). The (111) triplet is resolved in the INS spectra revealing translation-rotation coupling; in ascending order these three states are characterized by the TR quantum numbers $\lambda^{(a)} = 1$, $\lambda^{(b)} = 2$ and $\lambda^{(c)} = 0$.

Fig. 3 The INS spectrum of $H_2@C_{60}$ recorded on IN4C at 1.6 K. Incident neutron wavelength λ_n = 1.6 Å. This spectrum is integrated over the momentum transfer range $2 \leq \kappa \leq 8\,\text{Å}^{-1}$. Scattering from a sample comprising empty C_{60} cages has been subtracted.

Fig. 4. INS momentum transfer in $H_2@C_{60}$ recorded at 1.6 K with incident neutron wavelength λ_n = 1.1 Å: κ-dependence of (a) the rotational line in NE loss (14.7 meV), (b) the rotational line in NE gain (-14.7 meV), and c) the translational line in NE loss (22.5 meV). The solid lines are fits with the theoretical expressions; see text for details.

Fig. 5 $H_2@C_{60}$ at 1.6 K: Detail showing the fit to the translational line at 22.5meV (Jnl : 100 → 111) resolving the triplet structure arising from TR coupling. IN4C, λ_n = 1.6 Å.

Fig. 6 $H_2@C_{60}$ at 1.6K: IN4C spectra recorded with λ_n = 1.1 Å and λ_n = 1.2 Å. Scattering from a sample comprising empty C_{60} cages has been subtracted.

Fig. 7 $H_2@C_{60}$: IN5 spectra, in NE gain; λ_n = 5 Å. a) $T = 1.5$, 120 and 240 K. b) T = 240 K showing the peaks surrounding the rotational line that become populated with increasing temperature. Lower curve (x6); following subtraction of a quasi-elastic background modeled with a polynomial function. The tick marks identify the transition energies evaluated from the energy level diagram, Table 2 and Fig. 2. The triplet arising from TR coupling in the (111) state is resolved in these spectra; transitions are labeled with the participating state.

Fig. 8 $H_2@C_{60}$: IN5 (λ_n = 8 Å). Normalized amplitudes vs temperature of the (•) -14.7 and (□) -14.1 meV peaks. The solid lines represent the statistical weights of the initial states calculated using the Boltzmann distribution with degeneracies, $g_\lambda = 2\lambda + 1$, consistent with the assignment $\lambda^{(a)} = 1$, $\lambda^{(b)} = 2$ and $\lambda^{(c)} = 0$. The -14.7 meV peak

26

comprises two superimposed components and the dashed line represents the calculated amplitude assuming the transition matrix element ratio $\left|V_{\lambda^{(b)}}\right|^2 / \left|V_{\lambda^{(a)}}\right|^2 \simeq 0.4$ (see text for details).

Fig 9 The INS spectrum of HD@C_{60} evaluated by subtracting the spectrum of H_2@C_{60} from that of the mixed isotope sample (HD/H_2@C_{60}). IN4C: $T = 1.8$K, $\lambda_n = 1.6$ Å.

Fig 10 INS momentum transfer in HD@C_{60}. κ-dependence of (●) the rotational line (10.0 meV) and (□) the translational line (19.1 meV) both in NE loss. IN4C, $T = 1.6$K, $\lambda_n = 1.65$ Å.

Fig 11 INS spectrum of H_2@ATOCF at T=2.5K. The anisotropic cage potential lifts the three-fold degeneracies of both rotations and translations. The third translational peak at 30.2 meV is identified in this spectrum. IN4C, $\lambda_n = 1.24$ Å. (Inset: $\lambda_n = 1.8$ Å).

Fig 12 INS momentum transfer in H_2@ATOCF. κ-dependence of (●) the translational doublet centered on 17.5 meV and (□) the peak at 30.2 meV, both in NE loss, confirming the assignment of the latter to the third translational mode. Solid line: fit with Eqn. (5). IN4C, T=2.5K, $\lambda_n = 1.1$ Å.

References

[1] K. Komatsu, M. Murata and Y. Murata, Science **307**, 238 (2005)

[2] M. Murata, Y. Murata and K. Komatsu, J. Am. Chem. Soc. **128**, 8024 (2006)

[3] S. Mamone, J.Y.-C. Chen, R. Bhattacharyya, M.H. Levitt, R.G. Lawler, A.J. Horsewill, T. Rõõm, Z. Bačić and N.J. Turro, Coord. Chem. Rev. **255** 938 (2011)

[4] K. Kurotobi and Y. Murata, Science **333** 613 (2011)

[5] Y. Li, X. Lei, R.G. Lawler, Y. Murata, K. Komatsu and N.J. Turro, J. Phys. Chem. Lett. **1** 2135 (2010)

[6] G. Liu, Y. Wu and K. Porfyrakis, Curr. Org. Chem. **15** 1197 (2011)

[7] M. Murata, Y. Morinaka, K. Kurotobi, K. Komatsu and Y. Murata, Chem.Letters 39 (2010) 298

[8] K.E. Whitener, R.J. Cross, M. Saunders, S. Iwamatsu, S Murata, N. Mizorogi and S. Nagase, J. Am. Chem. Soc. **131** (2009) 6338

[9] C.M. Stanisky, R.J. Cross and M. Saunders, J. Am. Chem. Soc. **131** (2009) 339

[10] M. Murata, S. Maeda, Y. Morinaka, Y. Murata and K. Komatsu, J. Am. Chem. Soc. **130** 15800 (2008)

[11] N.J. Turro, A.A. Marti, J.Y.-C. Chen, S. Jockusch, R.G. Lawler, M. Ruzzi, E. Sartori, S.C. Chuang, K. Komatsu and Y. Murata, J. Am. Chem. Soc. **130** (2008) 10506

[12] M. Murata, Y. Murata and K. Komatsu, Chem. Comm. **46** 6083 (2008)

[13] S. Mamone, Min Ge, D. Hüvonen, U. Nagel, A. Danquigny, F. Cuda, M.C. Grossel, Y. Murata, K. Komatsu, M.H. Levitt, T. Rõõm and M. Carravetta, J. Chem. Phys. **130** 081103 (2009)

[14] Min Ge, U. Nagel, D. Hüvonen, T. Rõõm, S. Mamone, M.H. Levitt, M. Carravetta, Y. Murata, K. Komatsu, J.Y.-C. Chen and N.J. Turro, J. Chem. Phys. **134** 054507 (2011)

[15] Min Ge, U. Nagel, D. Hüvonen, T. Rõõm, S. Mamone, M.H. Levitt, M. Carravetta, Y. Murata, K. Komatsu, Xuegong Lei and N.J. Turro, J. Chem. Phys. **135** 114511 (2011)

[16] A.J. Horsewill, K.S. Panesar, S. Rols, M.R. Johnson, Y. Murata, K. Komatsu, S. Mamone, A. Danquigny, F. Cuda, S. Maltsev, M.C. Grossel, M. Carravetta and M.H. Levitt, Phys. Rev. Letters **102** 013001 (2009)

[17] A.J. Horsewill, S. Rols, M.R. Johnson, Y. Murata, M. Murata, K. Komatsu, M. Carravetta, S. Mamone, M.H. Levitt, J.Y.-C. Chen, J.A. Johnson, X. Lei and N.J. Turro, Phys. Rev. B **82** 081410(R) (2010)

[18] M. Carravetta, O.G. Johannessen, M.H. Levitt, I. Heinmaa, R. Stern, A. Samoson, A.J. Horsewill, Y. Murata and K. Komatsu, J. Chem. Phys. **124** 104507 (2006)

[19] M. Carravetta, A. Danquigny, S. Mamone, F. Cuda, O.G. Johannessen, I. Heinmaa, K.S. Panesar, R. Stern, M.C. Grossel, A.J. Horsewill, A. Samoson, M. Murata, Y. Murata, K. Komatsu and M.H. Levitt, Phys. Chem. Chem. Phys. **9** 4879 (2007)

[20] Y. Kohama, T. Rachi, J. Jing, Z. Li, J. Tang, R. Kumashiro, S. Izumisawa, H. Kawaji, T. Atake, H. Sawa, Y. Murata, K. Komatsu and K. Tanigaki, Phys. Rev. Letters **103** 073001 (2009)

[21] M. Xu, F. Sebastianelli, Z. Bačić, R. Lawler and N.J. Turro, J. Chem. Phys. **128** 011101 (2008)

[22] M. Xu, F. Sebastianelli, Z. Bačić, R. Lawler and N.J. Turro, J. Chem. Phys. **129** 064313 (2008)

[23] M. Xu, F. Sebastianelli, B.R. Gibbons, Z. Bačić, R. Lawler and N.J. Turro, J. Chem. Phys. **130** 224306 (2009)

[24] F. Sebastianelli, M. Xu, Z. Bačić, R. Lawler and N.J. Turro, J. Am. Chem. Soc. **132** 9826 (2010)

[25] R.J. Elliott and W.M. Hartmann, Proc. Phys. Soc. **90** 671 (1967)

[26] J.A. Young and J.U. Koppel, Phys. Rev. **135** A603 (1964)

[27] T. Yildirim and A.B. Harris, Phys. Rev. B **66** 214301 (2002)

[28] M. Xu, L. Ulivi, M. Celli, D. Colognesi and Z. Bačić, Phys. Rev. B **83** 241403(R) (2011)

[29] M. Xu and Z. Bačić, Phys. Rev. B **84** 195445 (2011)

[30] http://www.ill.eu/instruments-support/instruments-groups/yellowbook/

[31] S. Ye, M. Xu, Z. Bačić, R. Lawler and N.J. Turro, J. Phys. Chem. A **114** 9936 (2010)

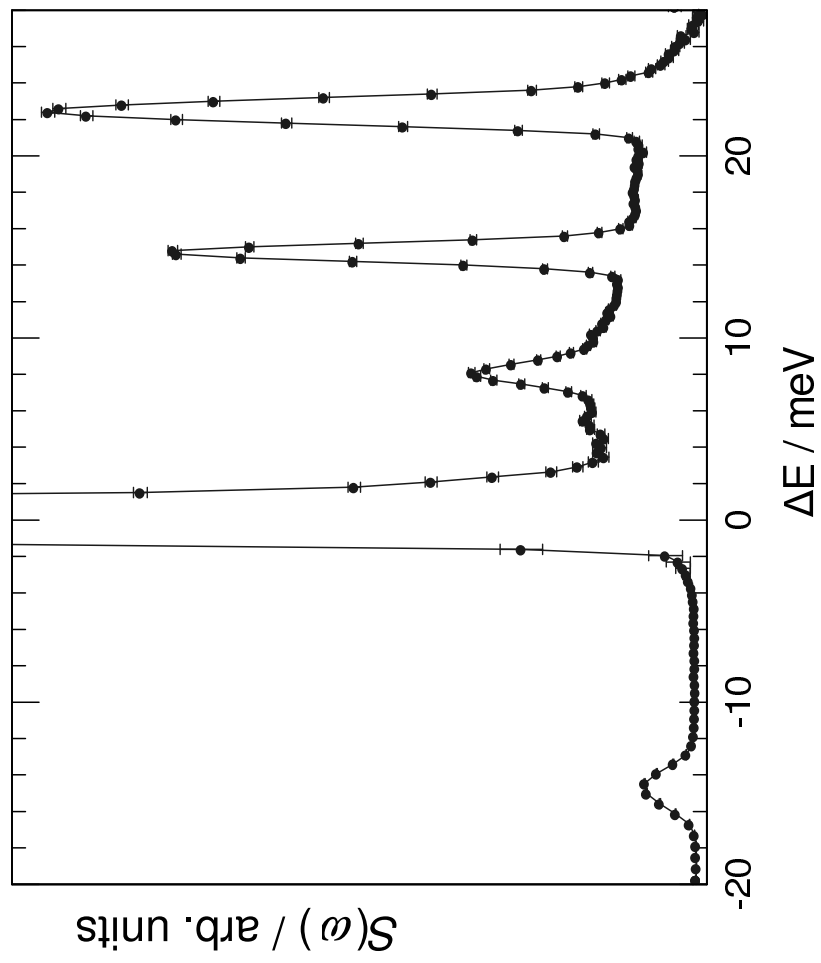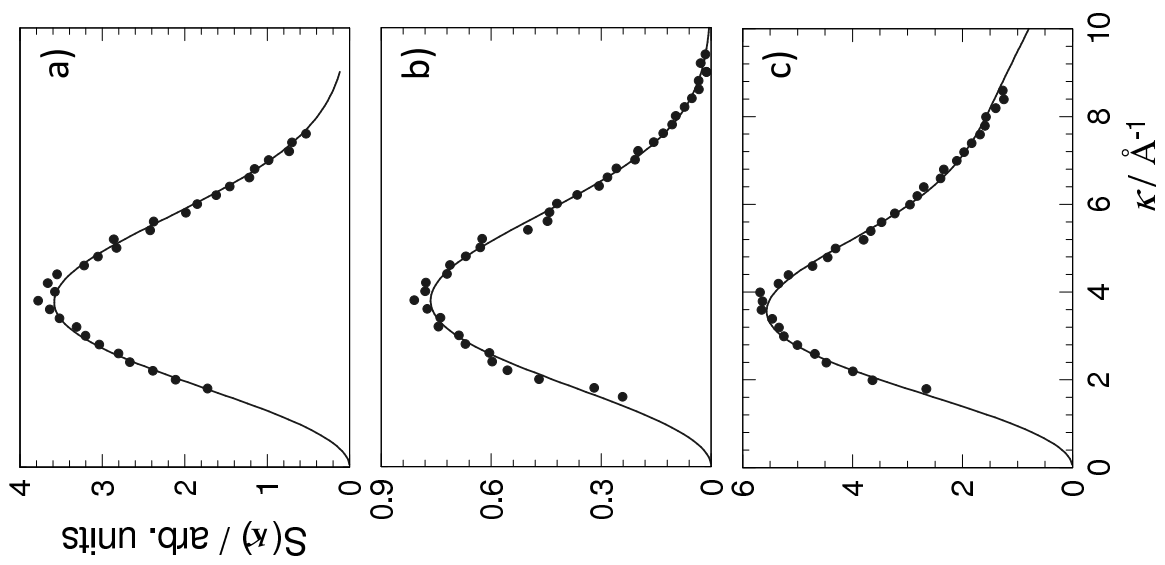HD@C$_{60}$

H$_2$@C$_{60}$

H$_2$@ATOCF
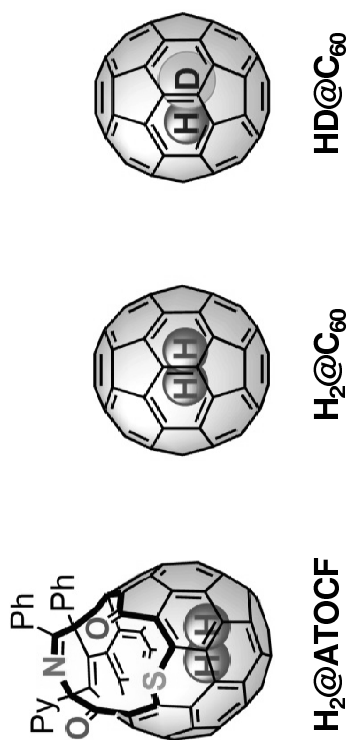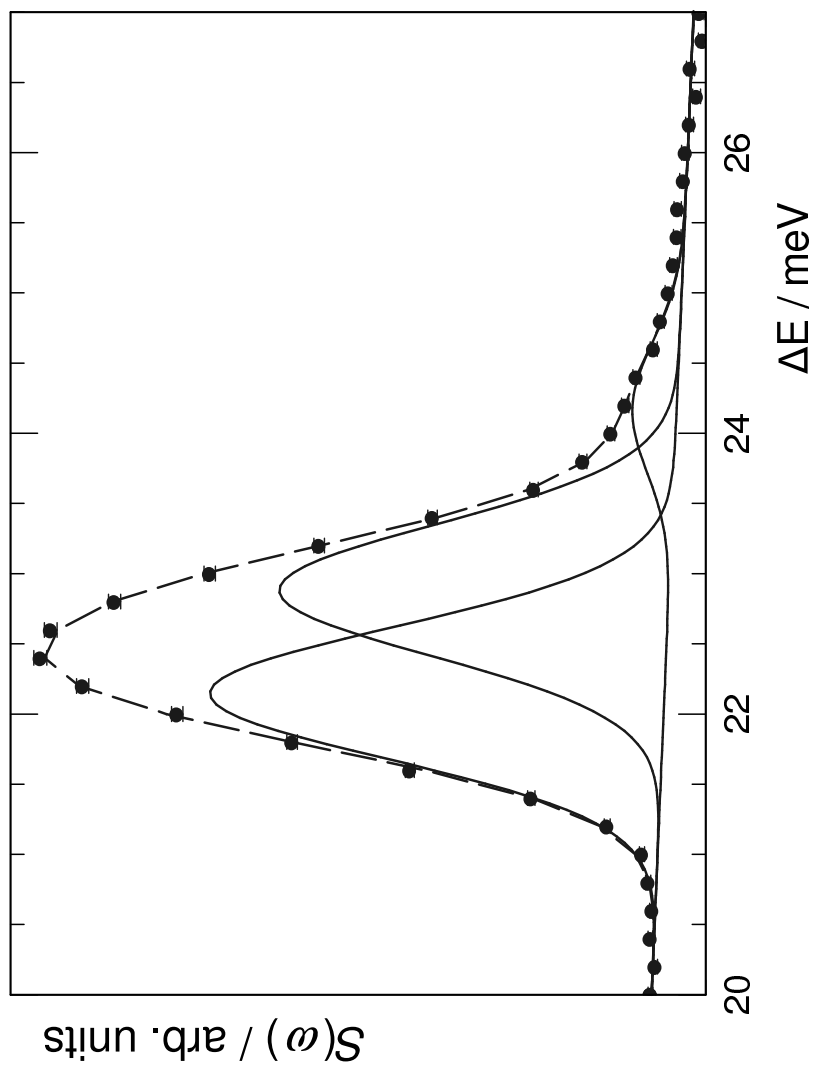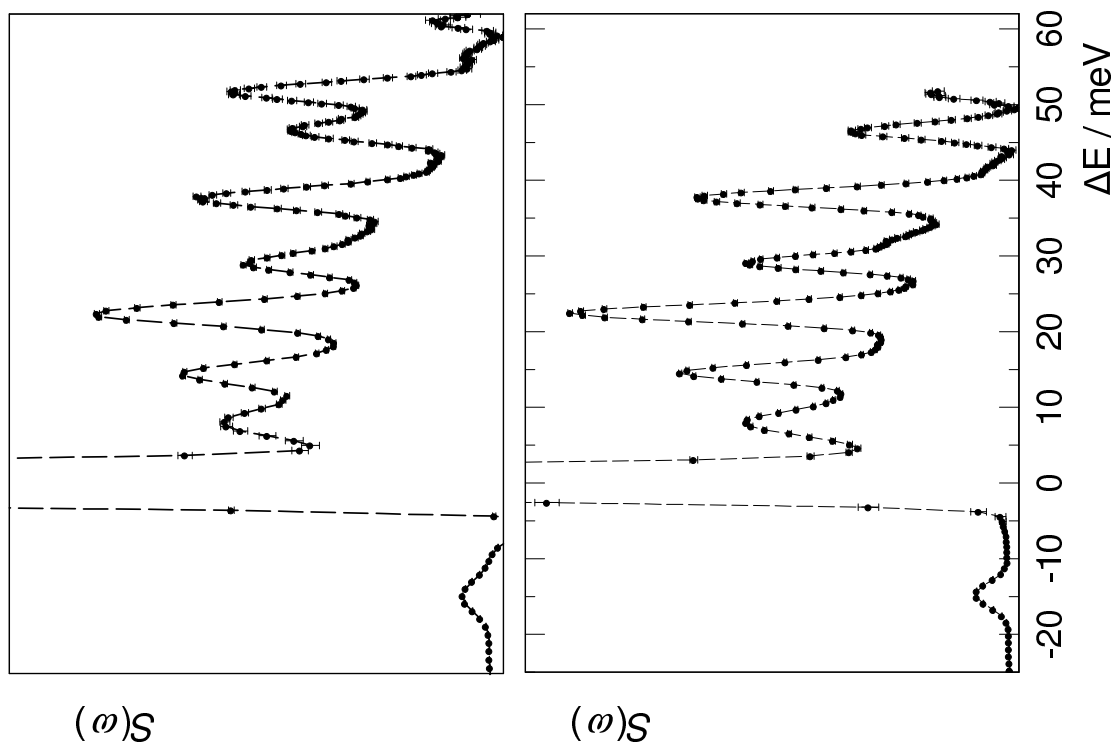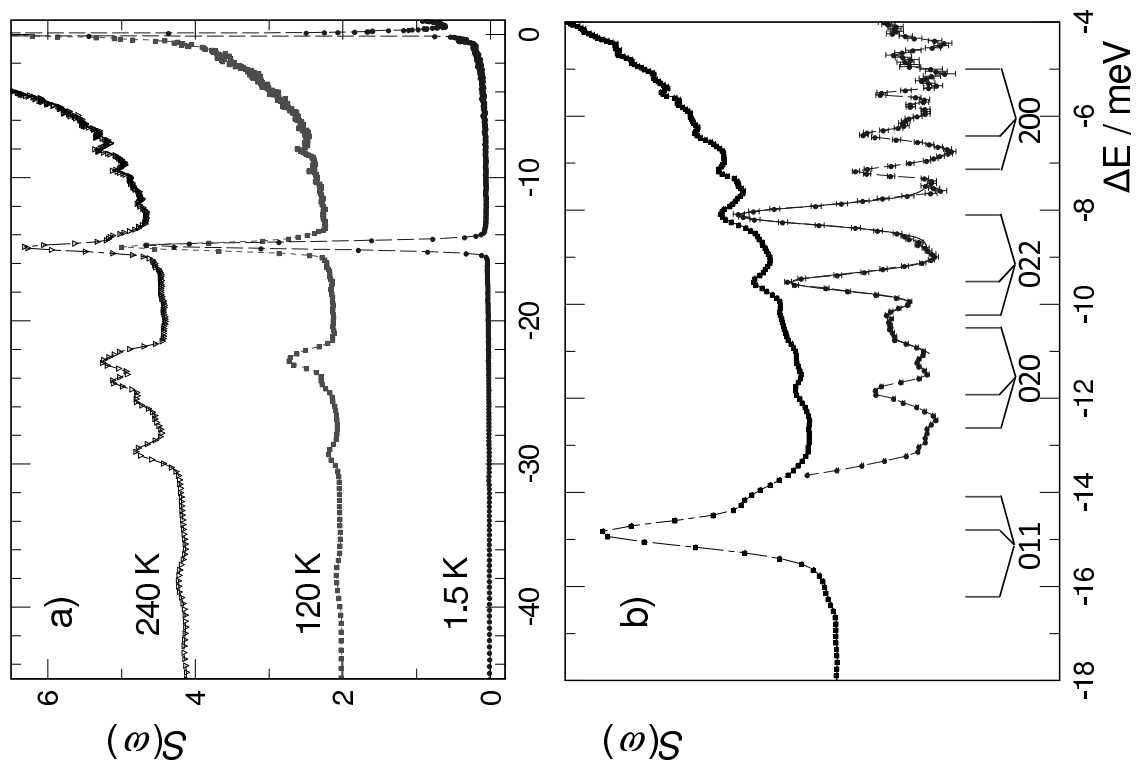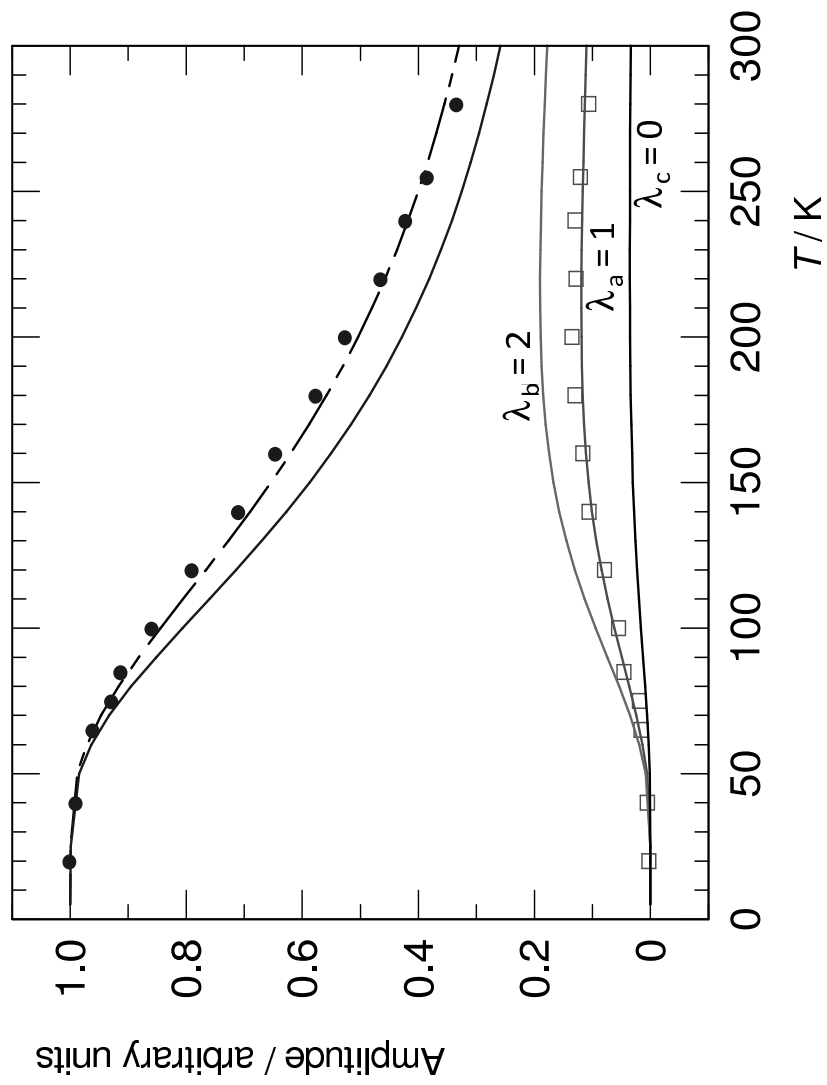
Figure 1   BR11640   11MAY2012
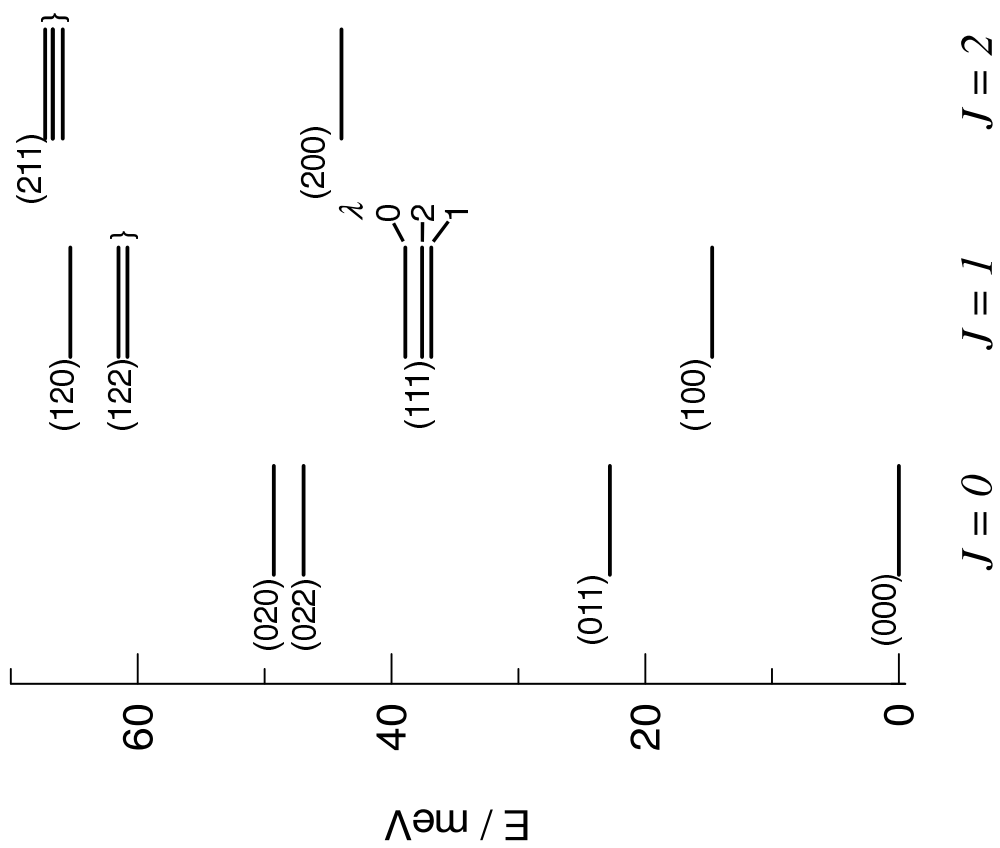
Figure 2   BR11640   11MAY2012

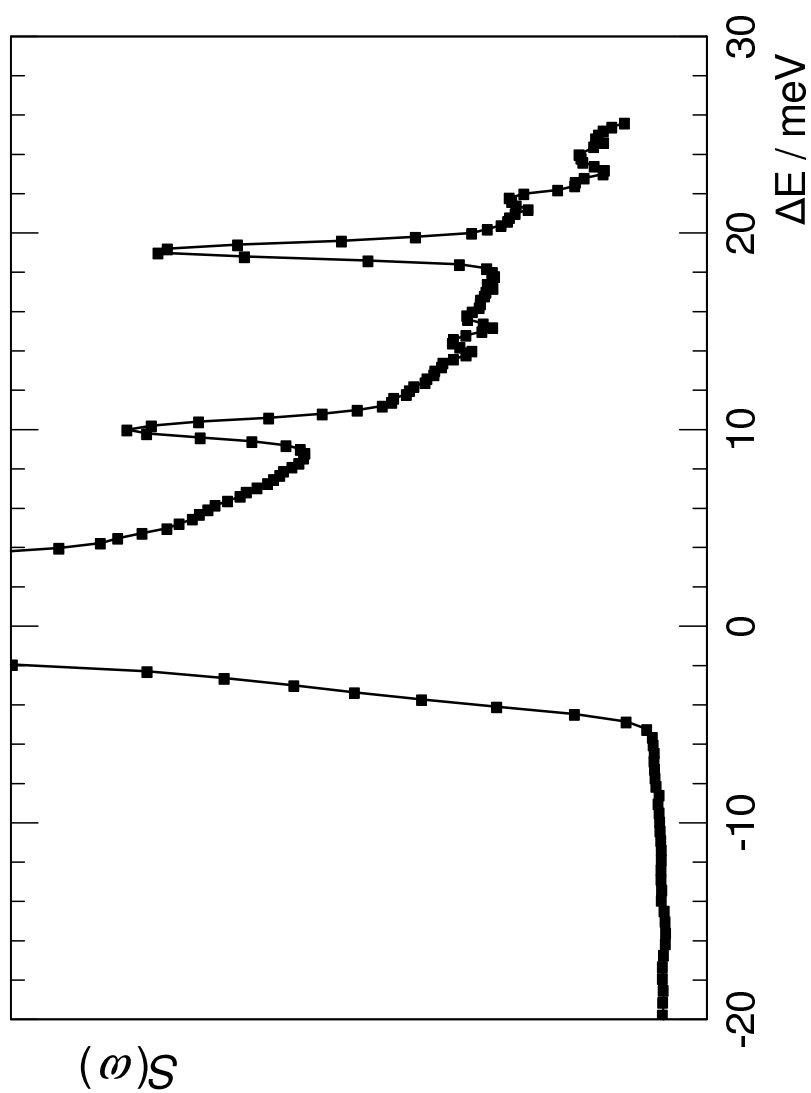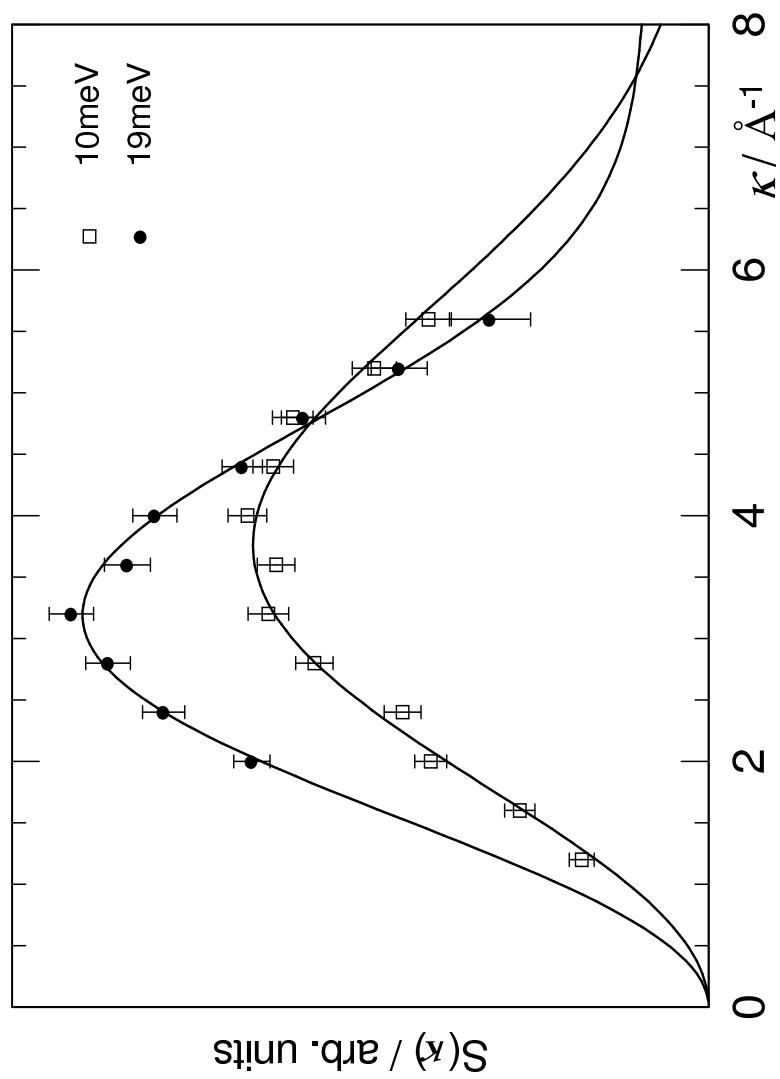Figure 3   BR11640   11MAY2012

Figure 4   BR11640   11MAY2012

Figure 5   BR11640   11MAY2012

$S(\omega)$

$S(\omega)$

ΔE / meV

Figure 6   BR11640   11MAY2012

Figure 7   BR11640   11MAY2012

Figure 8   BR11640   11MAY2012

Figure 9

BR11640   11MAY2012

Figure 10   BR11640   11MAY2012
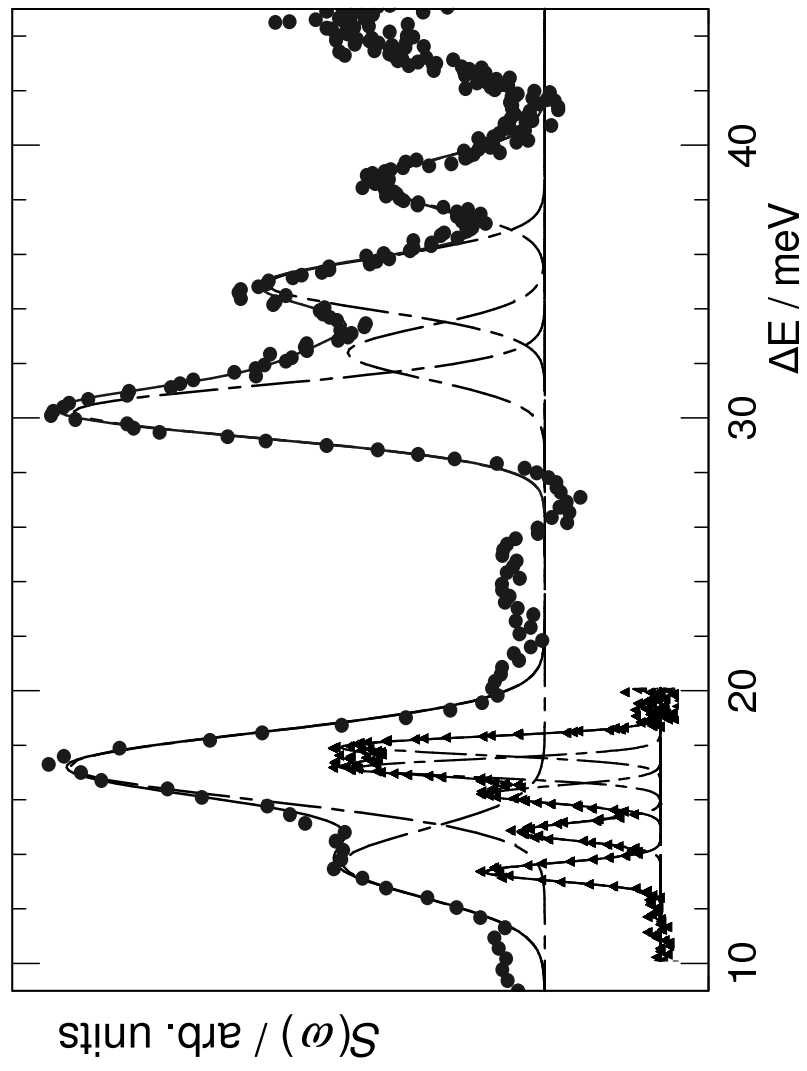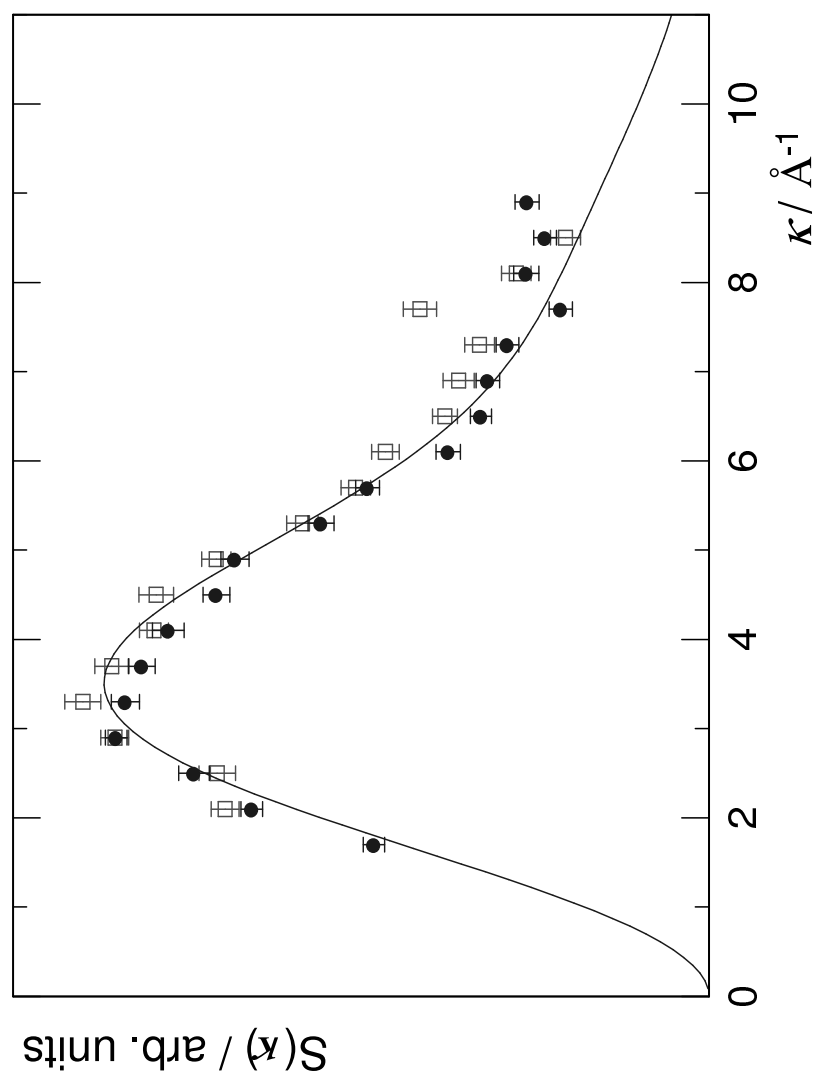
Figure 11   BR11640   11MAY2012

Figure 12   BR11640   11MAY2012